The effect of Base on the Facile Hydrothermal Preparation of Highly Active IrO_x Oxygen Evolution Catalysts

Jonathan Ruiz Esquius[a], David J. Morgan[a], Ioannis Spanos[b], Daniel G. Hewes,[a] Simon J. Freakley[c] and Graham J. Hutchings[a*]

[a] School of Chemistry, Cardiff Catalysis Institute, Cardiff University, Main Building, Park Place, Cardiff CF10 3AT, UK.

[b] Department of Heterogeneous Reactions, Max Planck Institute for Chemical Energy Conversion, Stiftstrasse 34-36, Muelheim an der Ruhr, 45470, Germany.

[c] Department of Chemistry, University of Bath, Claverton Down, Bath, BA2 2AY, UK.

* Hutch@cardiff.ac.uk

List of contents:

1. Catalyst characterisation

Ultraviolet – Visible Spectroscopy (UV-Vis)

UV-Vis was employed to monitor the conversion of $IrCl_3 \cdot 3H_2O$ (Sigma Aldrich) to amorphous iridium oxo-hydroxides using different bases (Li_2CO_3, LiOH, Na_2CO_3, NaOH, K_2CO_3 or KOH) following a hydrothermal synthesis. $Ir(H_2O)_3Cl_3$, $Ir(OH)_6^{3-}$ and the formation of Ir_nO_m oligomers can be observed at 400 nm, 320 nm and 580 nm respectively.[(1)] The IrO_x-base synthesis were performed in a 100 ml three-neck bottom flask with a reflux condenser attached to the middle neck, and rubber septa sealed the other two flask necks. Temperature was controlled using an oil bath and the solution was continuously stirred with the aid of a magnetic bar. 1 mmol of $IrCl_3$ and 8 mmol of base (Li_2CO_3, LiOH, Na_2CO_3, NaOH, K_2CO_3 or KOH) were dissolved in 40 ml of deionised water at 25 °C. Reaction aliquots were obtained by sampling 0.1 ml through the rubber septum using a syringe and diluting in a UV cuvette with 2 ml of deionised water. The synthetic protocol was divided in three distinct steps to facilitate data interpretation: Step 1 compromised stirring at 25 °C for 20 h, Step 2 consisted in heating the solution from 25 °C to reflux, Step 3 was the reflux of the reaction mixture for 3 h. In Step 2, the temperature was increased by 10 °C at a time, and the temperature was allowed to stabilise for 5 minutes before acquiring a UV-Vis spectra.

On one hand, for carbonate bases (Na_2CO_3 and K_2CO_3 in Figure S1a and S1c respectively), $Ir(H_2O)_3Cl_3$ is hydrolysed to $Ir(OH)_6^{3-}$ at 25 °C (Step 1), in order to observe Ir_nO_m oligomer formation heating to 85 °C - reflux is necessary. On the other hand, for hydroxide bases (NaOH and KOH in Figure S1b and S1d respectively), the formation of oligomers is observed after stirring at 25 °C for 20 h. However, to obtain IrO_x precipitation heating to 85 °C - reflux is as well required.

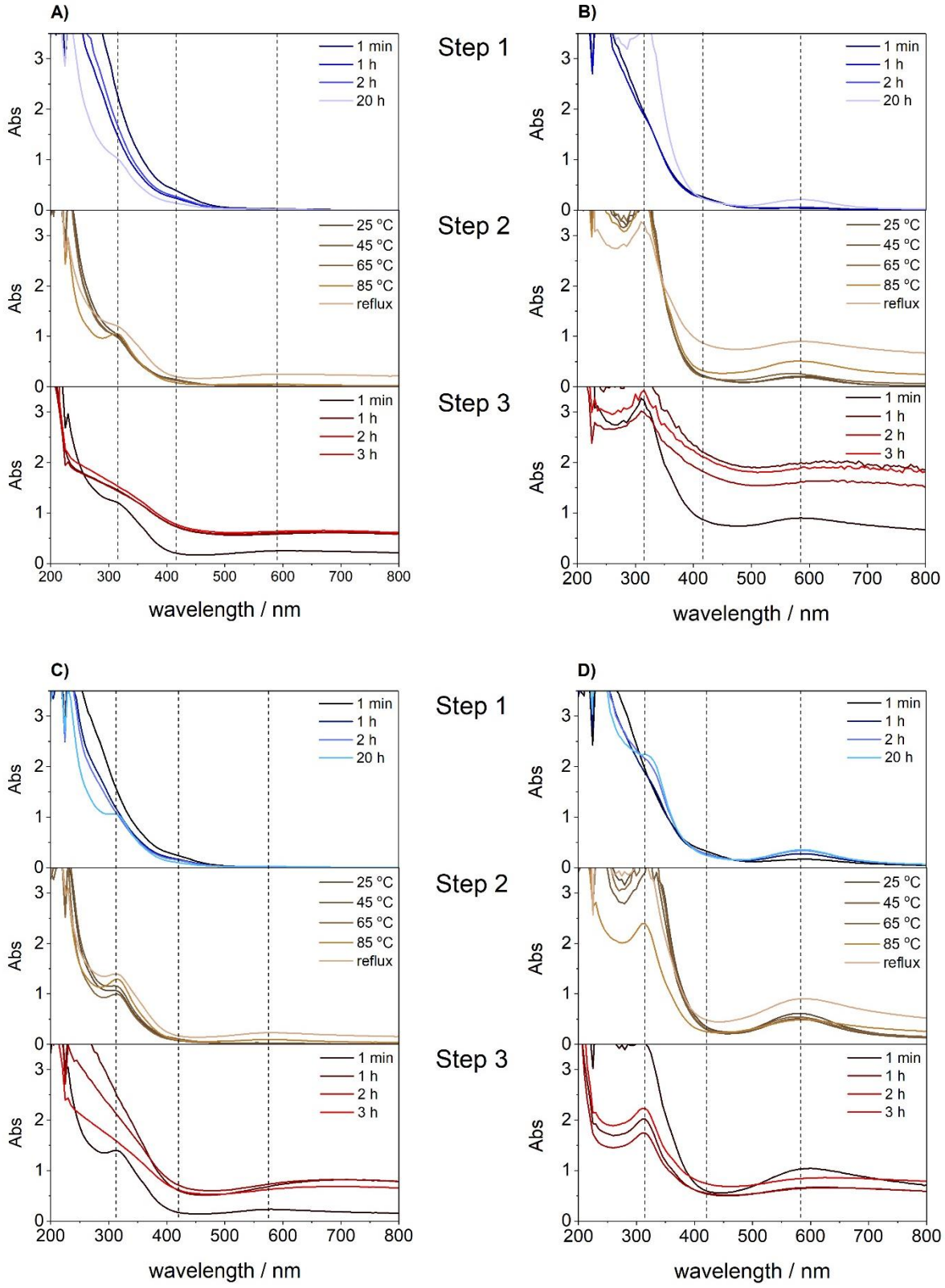

Figure S1. UV-Vis monitoring of the hydrothermal conversion of $IrCl_3$ to IrO_2 during step 1 (stirring at 25 °C for 20 h), step 2 (heat from 25 °C to reflux) and step 3 (reflux for 3 h) of the hydrothermal conversion of $IrCl_3$ to IrO_2 using a) Na_2CO_3 and b) NaOH c) K_2CO_3 d) KOH as a base.

X-ray powder diffraction (XRD)

XRD was used to analyse the crystalline phases present in the commercially sourced rutile IrO_2 (Sigma Aldrich, IrO_2-SA) and hydrate IrO_2 (Alfa Aesar, IrO_x-AA) standards (Figure S2). In good agreement with published characterisation for these materials,[2] only rutile (JCPDS-015-0876) was observed for IrO_2-SA, whilst metallic iridium (JCPDS-006-0598) was detected for IO_x-AA. According to Pfeifer *et al*.,[3] metallic iridium is present at the core of IrO_x-AA while IrO_x hydrated is localised at the outer layer.

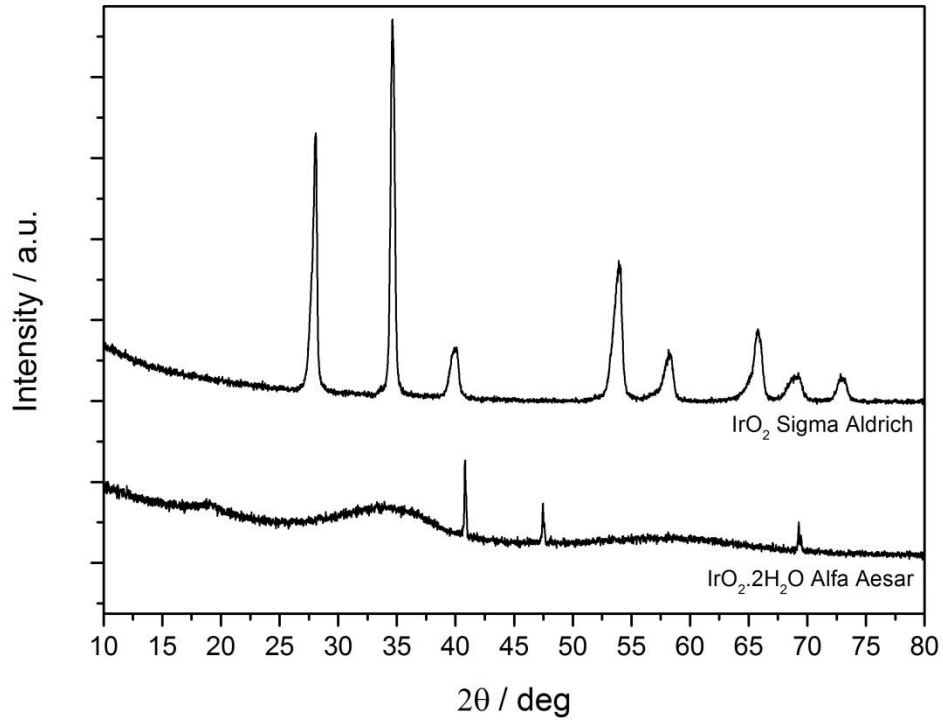

Figure S2. XRD pattern for commercial crystalline and amorphous IrO_2 samples from Sigma Aldrich and Alfa Aesar (Premion) respectively.

Raman spectroscopy

Raman spectroscopy was employed to confirm XRD characterisation, which suggested that synthesised IrO_x-base materials had no large order crystallinity. data acquisition was performed at 5 % laser intensity, 500 accumulations and 5 s of exposure time. A1g and Eg modes at 752 cm^{-1} and 561 cm^{-1} characteristic of rutile IrO_2[4,5,6] were observed for IrO_2-SA. Whilst the absence of these adsorption bands for IrO_x-AA and synthesised IrO_x-base catalysts confirmed the absence of rutile crystalline phase (Figure S3). The sharp peak at 459 cm^{-1}, 986 cm^{-1} and 1368 cm^{-1} correspond to artefacts generated from the silicon wafer.

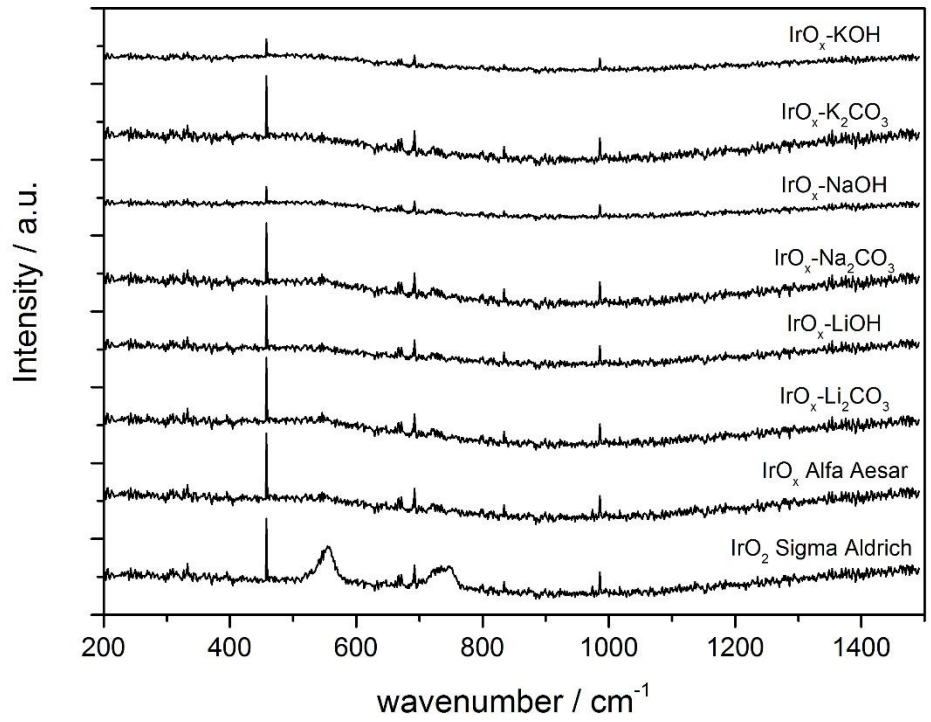

Figure S3. Raman spectroscopy for commercial standards and hydrothermally prepared IrO_x catalysts.

X-ray photoemission spectroscopy (XPS)

The peak fitting model developed by Morgan *et al*.[7] was used on the Ir(4f) and O(1s) spectra acquired for IrO_x-base catalysts. In figure 4a, the Ir(4f) of rutile IrO_2-SA and hydrate IrO_x-AA were compared. Rutile IrO_2 was centred at 61.9 eV, in accordance with being formed entirely of Ir(IV),[2,3] whilst IrO_x-AA was centred at 62.5 eV and showed a comparably broader peak envelope attributed to the presence of Ir(III) sites. Recorded Ir(4f) spectra for synthesised IrO_x-base catalysts (Figure S4) were shifted towards higher binding energy and broader than IrO_2-SA, comparable to commercial IrO_x-AA, indicating the presence of Ir(IV)/Ir(III) sites and in agreement with its amorphous structure.

The Ir/O ratio, obtained from the XPS quantification of Ir(4f) and O(1s), indicated an excess of oxygen compared to the stoichiometric oxide (Table S1). The excess of oxygen observed from the Ir/O ratio can be explained by the presence of surface hydroxide and water/carbonates at 531.1 eV and 532.4 eV respectively, apart from the oxide presence detected at 530.2 eV (Figure S5).

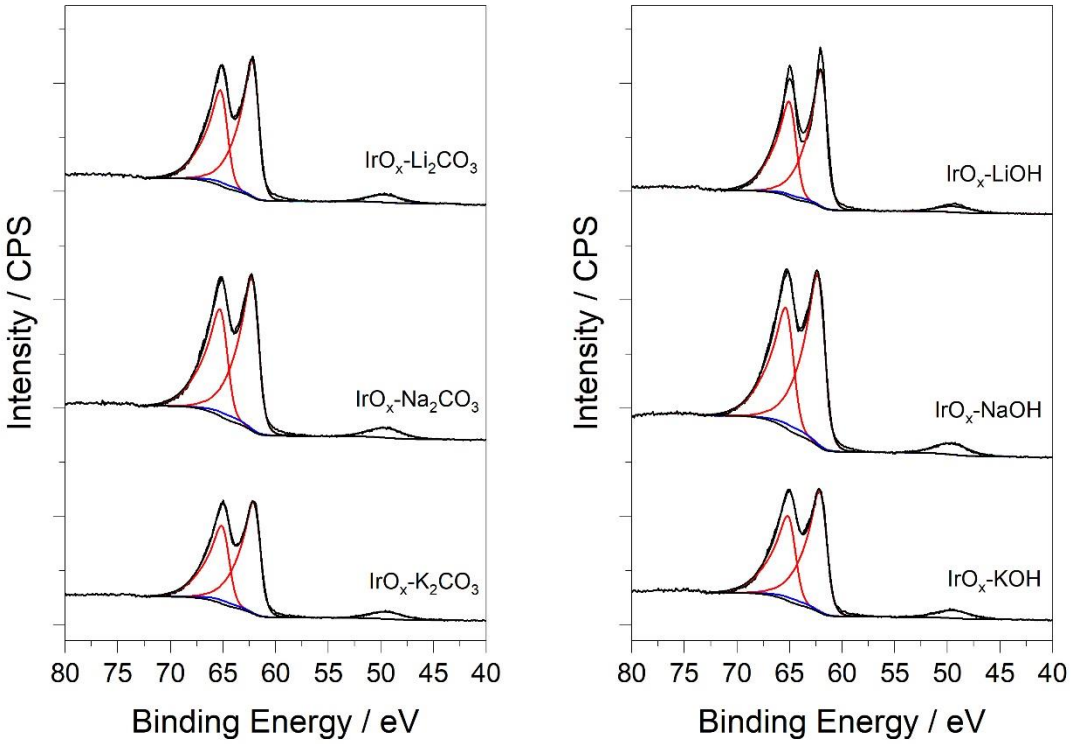

Figure S4. Ir(4f) XPS spectra for hydrothermally prepared synthesised IrO_x catalysts. Red and blue fittings correspond to Ir(4f) and Ir(5p) respectively.

Table S1. Ir/O ratio obtained from the XPS quantification of the Ir(4d) and O(1s) peaks.

Catalyst	Ir/O ratio	Catalyst	Ir/O ratio
IrO_2 Sigma Aldrich	0.49	IrO_2 Alfa Aesar	0.31
IrO_2-Li_2CO_3	0.32	IrO_2-LiOH	0.32
IrO_2-Na_2CO_3	0.29	IrO_2-NaOH	0.33
IrO_2-K_2CO_3	0.33	IrO_2-KOH	0.33

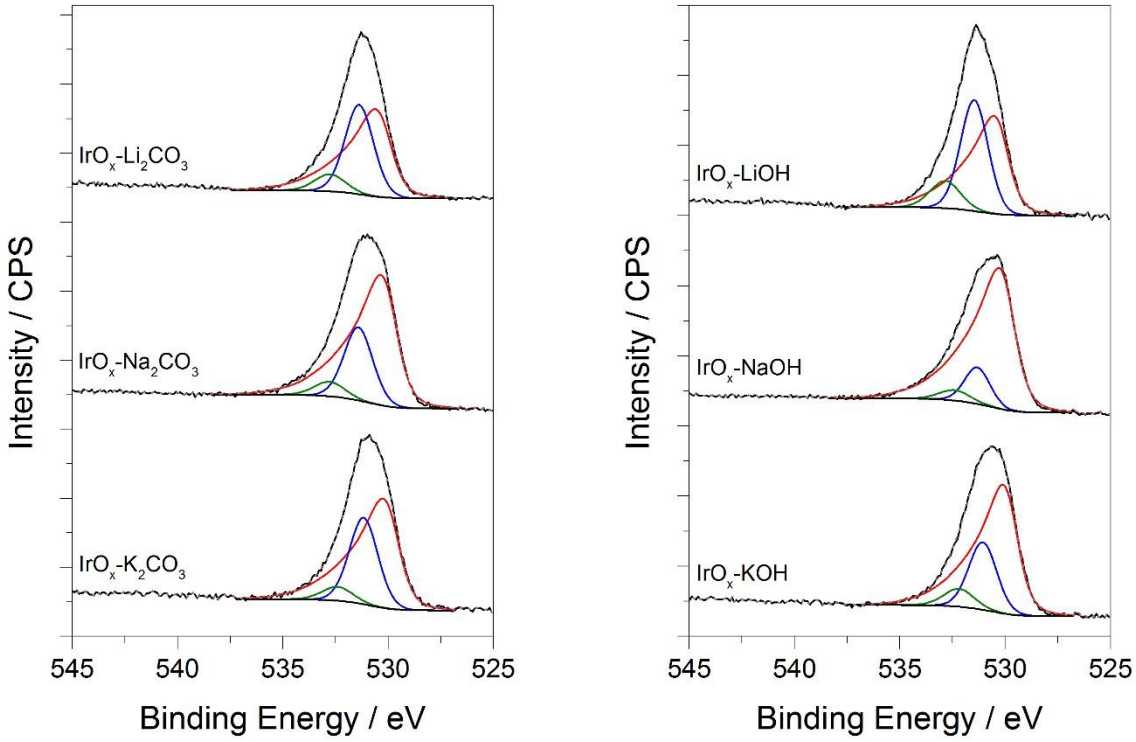

Figure S5. O(1s) XPS spectra for hydrothermally prepared IrO_x catalysts using different bases. Oxide, hydroxide and water components are represented with red, blue and green lines respectively.

2. Electrochemical measurements

Electrochemically active surface area (ECSA) normalised activity

Intrinsic catalytic activity of hydrothermally prepared IrO_x catalysts was obtained by LSV and normalised to the geometric surface area (figure 5 in main text). To confirm the higher activity of IrO_x-Li_2CO_3 compared to IrO_x-LiOH and IrO_x-AA, intrinsic activities were normalised against the roughness factor, obtained from ECSA measurements,[8] and to the iridium mass.

ECSA measurements were performed on IrO_x-Li_2CO_3, IrO_x-LiOH and IrO_x-AA catalysts to evaluate the electrochemically available surface area during OER. To avoid the interference of Faradaic processes, cyclic voltammetry (CV) between 0.5 V_{RHE} and 0.6 V_{RHE} with scan rates at 2 $mV \cdot s^{-1}$, 5 $mV \cdot s^{-1}$, 10 $mV \cdot s^{-1}$, 50 $mV \cdot s^{-1}$ and 100 $mV \cdot s^{-1}$ were measured (Figure S6a). The slope obtained from plotting the average between the maximum anodic current density and the minimum cathodic current density, $(J_{max,\,an} - J_{min,\,cat})/2$, against the scan rate is the double layer capacitance (C_{DL}) of the catalyst (Figure S6b).

The double layer capacitance can then be converted to the electrochemically active surface area by diving it by the specific capacitance in acidic conditions ($C_{s,\,ac.}$ = 0.035 mF·cm^{-2}).

$$ECSA = C_{DL} / C_{s,\,ac}$$

ECSA values of 0.014 cm^{-2}, 0.001 cm^{-2} and 0.037 cm^{-2} were obtained for IrO_x-Li_2CO_3, IrO_x-LiOH and IrO_x-AA respectively. The roughness factor (R_f) of each catalyst can be obtained by diving ECSA with the geometric surface area of the electrode (in this case 0.196 cm^2). The measured R_f for IrO_x-Li_2CO_3, IrO_x-LiOH and IrO_x-AA was 0.073, 0.044 and 0.190 respectively. Normalised activities with R_f confirmed the higher activity of IrO_x-Li_2CO_3 compared to IrO_x-LiOH and IrO_x-AA (Figure S6c).

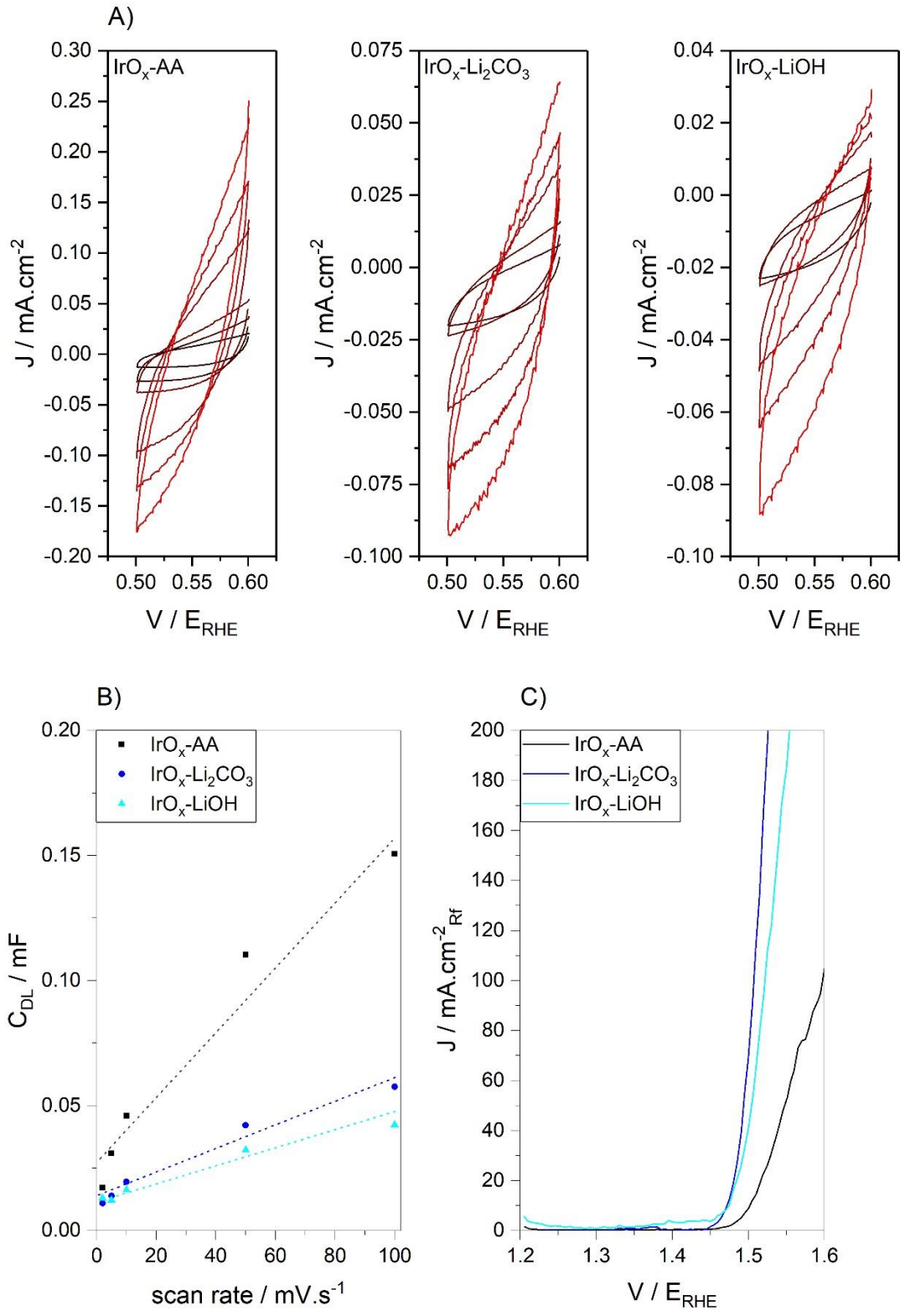

Figure S6. a) Double-layer capacitance measurements for the determination of ECSA, b) J_{cat}-J_{an} ploted against CV scan rate and c) roughness factor normalised activities for IrO_x-AA, IrO_x-Li_2CO_3 and IrO_x-LiOH.

Iridium mass normalised activity towards OER

In this work, the catalyst concentration on the working electrode was kept constant at 100 $\mu g_{cat} \cdot cm^{-2}$. Electrode surface area normalised activity for OER measured by LSV indicated the higher activity of IrO_x-Li_2CO_3 compared to commercial IrO_x-AA, and the rest of prepared IrO_x catalysts. The main drawback against normalising OER catalyst activity to the electrode surface area is its dependence on the catalyst loading. Moreover, the determination of the ECSA, and the roughness of a catalyst, are subject to inaccuracies, which can vary on several orders of magnitude.[7] As discussed by Fabbri *et. al.*[9] it is best to normalise catalyst activity against the iridium mass loading. To determine the mass of iridium on the electrode thermogravimetric analysis (TGA) was performed on all catalysts (Figure S7a). TGA were recorded on a PerkinElmer TGA 4000 instrument under N_2 (from 30 °C to 650 °C at 5 $°C \cdot min^{-1}$). The corresponding mass loss was assigned to surface hydroxide groups and to physisorbed water, which yielded rutile IrO_2. Through TGA results, the catalyst loading on the electrode (100 $\mu g_{cat} \cdot cm^{-2}$) was converted to the iridium mass on the electrode and used to normalise the OER activity. Iridium mass normalised activities (Figure S7b) confirmed the higher activity of IrO_x-Li_2CO_3 for OER compared to the other catalysts.

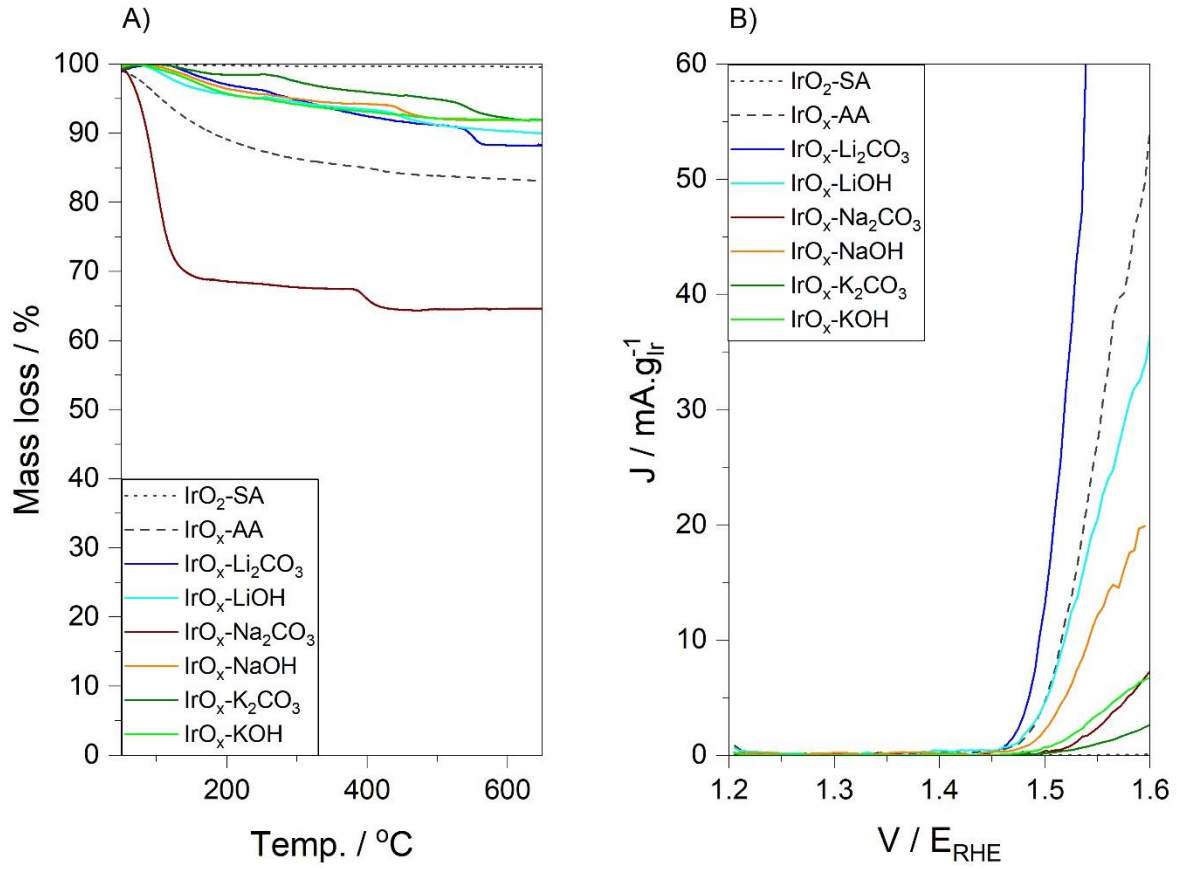

Figure S7. a) Mass loss obtained from TGA for synthesised IrO_x and commercial IrO_2 standards; b) Iridium mass normalised activity for OER catalysts.

Tafel slope

The slope obtained from plotting the ohmic drop corrected overpotential against the logarithm of the current density, described as Tafel slope, is an empirical parameter that contains information about the electrocatalytic activity and the reaction mechanism.[9,10] By comparing the experimental Tafel slope with theoretical calculations the rate determining step of the reaction can be elucidated. To correlate if differences in activity observed by LSV for IrO_x-AA, IrO_x-Li_2CO_3 and IrO_x-LiOH catalysts can relate with different rate determining step during OER Tafel slopes were measured (Figure S8). Tafel slopes were derived from semi-steady-state conditions obtained from LSV measurements performed at a ramp rate of 0.5 mV·s^{-1}. At low overpotential, measured Tafel slopes for IrO_x-AA, IrO_x-Li_2CO_3 and IrO_x-LiOH were 37 mV·dec^{-1}, 38 mV·dec^{-1}, and 35 mV·dec^{-1} respectively, in agreement with previously reported values (~ 40 mV·dec^{-1}).[10,11,12,13] Indicating that different activity observed between catalysts are not attributed to differences in the OER rate determining step.

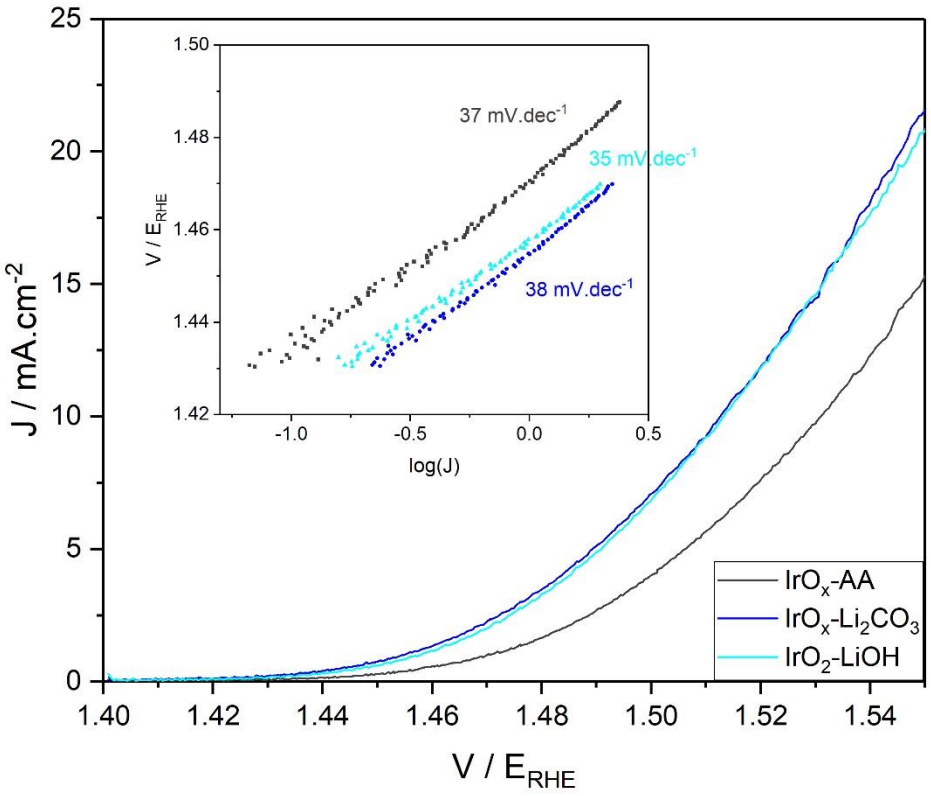

Figure S8. Semi-steady-state LSV polarization curves recorded between 1.4 V_{RHE} and 1.55 V_{RHE} at 0.5 $mV \cdot s^{-1}$ for IrO_x-AA, IrO_x-Li_2CO_3 and IrO_x-LiOH catalysts and obtained Tafel plots at low overpotential (1.43 V_{RHE} - 1.47 V_{RHE}).

Li^+, Na^+ and K^+-doped Rutile IrO_2

To confirm that lithium is acting as a promoter IrO_x catalyst for OER, rutile IrO_2 from Sigma Aldrich was doped with Li^+, Na^+ and K^+. Gao *et.al.*(11) doped rutile IrO_2 by its reaction with LiOH, NaOH and KOH at 300 °C. After reaction the surface of IrO_2 hydrolysed resulting in enhanced activity, nevertheless, the material doped with lithium showed higher activity compared to sodium and potassium towards OER, which was attributed to the higher promoting effect of lithium.

Since in the present work heat treatment was avoided, cation doping (Li^+, Na^+ or K^+) was achieved during the catalyst ink preparation. For the catalyst ink preparation 5 mg of rutile IrO_2 was re-dispersed in 1.23 ml of 0.1 M alkaline aqueous solution (LiOH, NaOH or KOH), 1.23 ml of ethanol and 40 µl of nafion solution. The catalyst ink was sonicated for 30 min to ensure a homogenous dispersion, and then 10 µl of the catalyst ink was drop-cast in the working electrode and dried under a N_2 flow for 30 min. Doped-rutile IrO_2 catalyst showed higher

catalytic activity than rutile IrO_2-SA (Figure S9a), which can be attributed to the formation of surface hydroxide groups formed after alkaline treatment during the catalyst ink preparation. Nevertheless, higher activity was observed for Li^+-doped rutile IrO_2 compared to Na^+ or K^+-doped rutile IrO_2, in line with the higher promoting effect of lithium.

To ensure that improved activity for OER, a part from the promoting effect of ink preparation in alkaline condition sand concomitant IrO_2 surface hydroxylation, is related to the presence of Li^+, a IrO_2-SA electrode was prepared in standard conditions (1.23 ml H_2O, 1.23 mL ethanol, 40 µl nafion solution) and measured in a standard 3-electrode cell (40 ml, 0.1 M $HClO_4$) by LSV (1.2 V_{RHE} - 1.7 V_{RHE}, 5 $mV \cdot s^{-1}$). Catalytic activity for OER was measured after consecutive 0.5 ml addition of 0.1 M LiOH by LSV. As observed in Figure S9b, improved current density by LSV was measured after each consecutive addition. In acids conditions, the OER mechanism is not dependent on the reaction pH,[14] and hence, improved activity more likely relates with the presence of Li^+. Nevertheless, further research is needed to understand whether lithium is acting as a promoter, changing the local structure of rutile IrO_2 forming active motifs or just increasing the population of active sites.

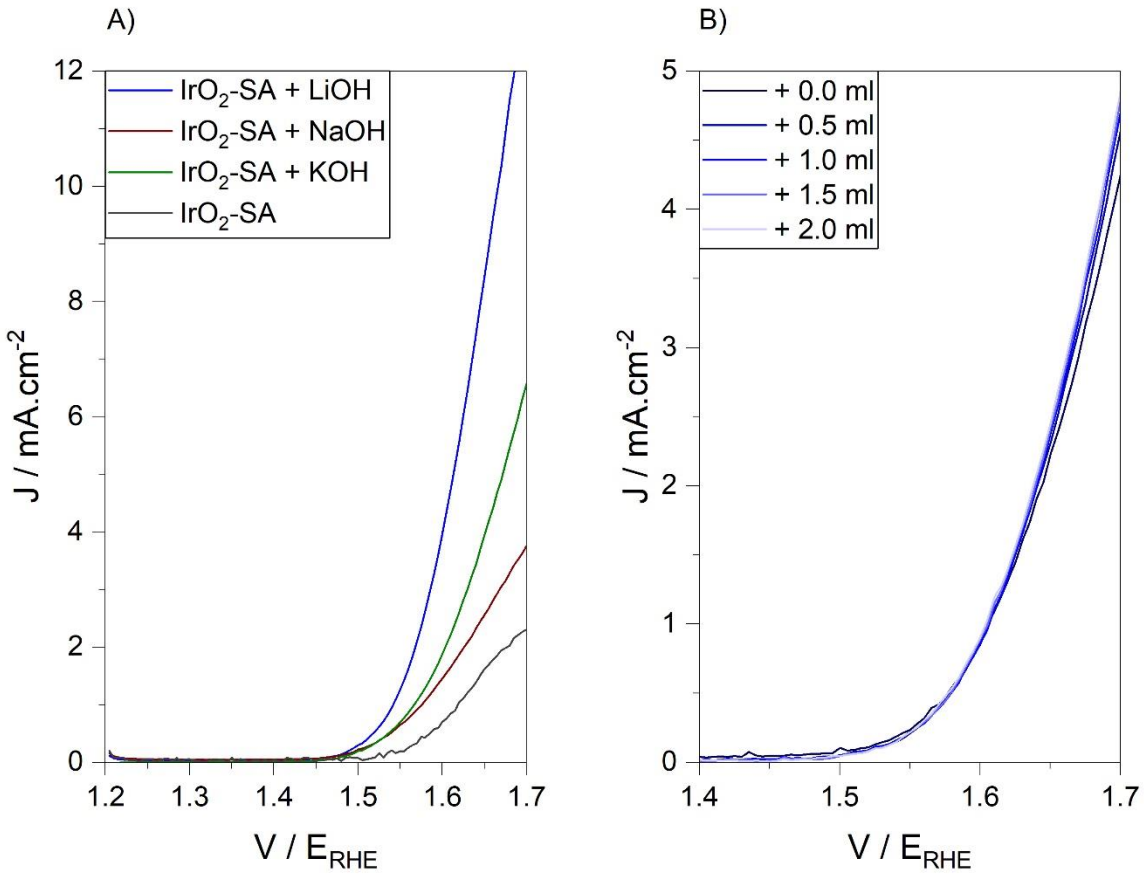

Figure S9. IrO_2-SA catalytic activity towards OER determined by LSV (1.2 V_{RHE} – 1.7 V_{RHE}, 5 $mV \cdot s^{-1}$) for a) catalyst ink containing 0.1 M solution of LiOH, NaOH or KOH. b) addition of 0.1 M LiOH into the electrolyte.

Catalyst deactivation towards OER

The electrochemical assessment of IrO_x catalysts for OER in $HClO_4$ 0.1 M was performed in a 3-electrode flow cell described previously in literature.[8] Intrinsic catalytic activity was assessed by LSV (1.2 V_{RHE} to 1.7 V_{RHE} at 5 $mV \cdot s^{-1}$) at the beginning of the experiment. Rutile IrO_2 showed no significant current density in the potential range studied. It was observed that IrO_x-NaOH, IrO_x-Na_2CO_3, IrO_x-KOH or IrO_x-K_2CO_3 performed poorly compared to commercial IrO_x-AA. IrO_x-LiOH showed comparable intrinsic activity to the commercial IrO_x-AA (1.52 V_{RHE} at 22 $mA \cdot cm^{-2}$), whilst IrO_x-Li_2CO_3 (1.50 V_{RHE} at 22 $mA \cdot cm^{-2}$) outperformed the commercial IrO_2-AA standard.

To determine the catalyst degradation occurred during CP (2 h, 10 $mA \cdot cm^{-2}$), the potential to reach a 22 $mA \cdot cm^{-2}$ current density by LSV before and after CP were compared (Figure S10). Catalysts in which glassy carbon corrosion was observed during CP, showed no activity in the consecutive LSV measurement. The catalytic activity of IrO_2-LiOH was seriously compromised

after CP, and the current density measured by LSV did not reach 22 mA·cm^{-2}. IrO_2-Li_2CO_3 showed a potential increase of only 38 mV after CP compared to 80 mV for commercial IrO_2-AA.

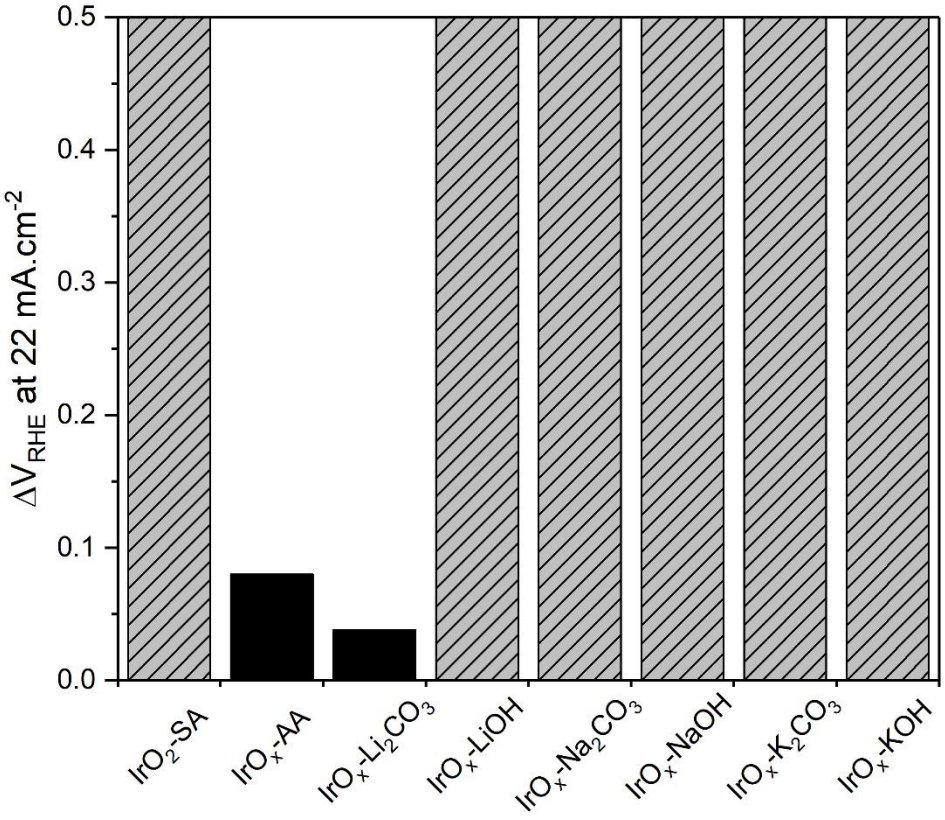

Figure S10. Increase in the potential measured by LSV at a current density of 22 mA·cm^{-2} before and after CP (2 h, 10 mA·cm^{-2}).

Iridium dissolution was measured with an ICP coupled to the electrochemical flow cell in the Max Planck Institute for Chemical Energy Conversion in Germany, as reported previously.[8] Hydrous IrO_x (Alfa Aesar) and IrO_x-Li_2O_3 were drop coated in an Au (0.196 cm^2) electrode instead of a glassy carbon, used in previous measurements. The conversion of the recorded ICP signal to the iridium monolayers·s^{-1} was done as follows: The ICP sensitivity for Ir is 1 ppb, with a 2 h CP experiment at 0.86 ml·min^{-1} the ICP sensitivity is 0.014 ng_{Ir}·s^{-1} or 2.2x10^{-5} monolayers·s^{-1}.

References

1. Xu, D.; Diao, P.; Jin, T.; Wu, Q.; Liu, X.; Guo, X.; Gong, H.; Li, F.; Xiang, M.; Ronghai, Y. Iridium Oxide Nanoparticles and Iridium/Iridium Oxide Nanocomposites: Photochemical Fabrication and Application in Catalytic Reduction of 4-Nitrophenol, *ACS Applied Materials & Interfaces*, **2015**, *7* (30), 16738-16749.

2. Pfeifer, V.; Jones, T. E.; Velasco Vélez, J. J.; Massué, C.; Arrigo, R.; Teschner, D.; Girgsdies, F.; Scherzer, M.; Greiner, M. T.; Allan, J.; Hashagen, M.; Weinberg, G.; Piccinin, S.; Hävecker, M.; Knop-Gericke, A.; Schlögl, R. The electronic structure of iridium and its oxides, *Surface and Interface Analysis*, **2016**, *48* (5), 261-273.

3. Pfeifer, V.; Jones, T. E.; Velasco Velez, J. J.; Massué, C.; Greiner, M. T.; Arrigo, R.; Teschner, D.; Girgsdies, F.; Scherzer, M.; Allan, J.; Hashagen, M.; Weinberg, G.; Piccinin, S.; Hävecker, M.; Knop-Gericke, A.; Schlögl, R. The electronic structure of iridium oxide electrodes active in water splitting, *Physical Chemistry Chemical Physics*, **2016**, *18* (4), 2292-2296.

4. Musić, S.; Popović, S.; Maljković, M.; Skoko, Z.; Furić, K.; Gajović, A. Thermochemical formation of IrO_2 and Ir, *Materials Letters*, **2003**, *57* (29), 4509-4514.

5. Audichon, T.; Guenot, B.; Baranton, S.; Cretin, M.; Lamy, C.; Coutanceau, C. Preparation and characterization of supported $Ru_xIr_{(1-x)}O_2$ nano-oxides using a modified polyol synthesis assisted by microwave activation for energy storage applications, *Applied Catalysis B: Environmental*, **2017**, *200*, 493-502.

6. Liao, P. C.; Chen, C. S.; Ho, W. S.; Huang, Y. S.; Tiong, K. K. Characterization of IrO_2 thin films by Raman spectroscopy, *Thin Solid Films*, **1997**, *301* (1), 7-11.

7. Freakley, S. J.; J. Esquius, J. R.; Morgan, D. J. The X-ray photoelectron spectra of Ir, IrO_2 and $IrCl_3$ revisited, *Surface and Interface Analysis*, **2017**, *49* (8), 794-799.

8. Spanos, I.; Auer, A. A.; Neugebauer, S.; Deng, X.; Tüysüz, H.; Schlögl, R. Standardized Benchmarking of Water Splitting Catalysts in a Combined Electrochemical Flow Cell/Inductively Coupled Plasma-Optical Emission Spectrometry (ICP-OES) Setup, *ACS Catalysis*, **2017**, 7, 3768-3778.

9. Fabbri, E.; Habereder, A.; Waltar, K.; Kötz, R. T. J. Schmidt, Developments and perspectives of oxide-based catalysts for the oxygen evolution reaction, *Catalysis Science and Technology,* **2014**, 4 (11), 3800-3821.

10. Shinagawa, T.; Garcia-Esparza, A. T.; Takanabe, K. Insight on Tafel slopes from a microkinetic analysis of aqueous electrocatalysis for energy conversion, *Scientific reports*, **2015**, 5, 13801.

11. Gao, J.; C. Xu, C. Q.; Hung, S. F.; Liu, W.; Cait, W.; Zeng, Z.; Jia, C.; Chen, H. M.; Xiao, H.; Li, J.; Huang, Y.; Liu, B. Breaking Long-Range Order in Iridium Oxide by Alkali Ion for Efficient Water Oxidation, *Journal of the American Chemical Society*, **2019**, 141 (7), 3014-3023.

12. Ouattara, L.; Fierro, S.; Frey, O.; Koudelka, M.; Comninellis, C. Electrochemical comparison of IrO_2 prepared by anodic oxidation of pure iridium and IrO_2 prepared by thermal decomposition of H_2IrCl_6 precursor solution, *Journal of Applied Electrochemistry*, **2009**, 39 (8), 1361-1367.

13. Fierro, S.; Kapalka, A.; Comniellis, C. Electrochemical comparison between IrO_2 prepared by thermal treatment of iridium metal and IrO_2 prepared by thermal decomposition of H_2IrCl_6 solution, *Electrochemistry Communications*, **2010**, 12 (1), 172-174.

14. Giordano, L.; Han, B.; Risch, M.; Hong, W. T.; Rao, R. R.; Stoerzinger, K. A.; Shao-Horn, Y. pH dependence of OER activity of oxides: Current and future perspectives, *Catalysis Today*, **2016**, 262, 2-10.